SIMULTANEOUS INVERSION OF 3D SEISMIC DATA FROM A WOLFCAMPIAN LIMESTONE RESERVOIR IN THE EASTERN SHELF OF THE PERMIAN BASIN, U.S.A.

JACK D. DEANS and GEORGE A. MCMECHAN

Center for Lithospheric Studies, The University of Texas at Dallas, 800 W. Campbell Road, Richardson, TX 75080-3021, U.S.A.

(Received November 11, 2011; revised version accepted March 2, 2012)

ABSTRACT

Deans, J.D. and McMechan, G.A., 2012. Simultaneous inversion of 3D seismic data from a Wolfcampian reservoir in the eastern shelf of the Permian Basin, U.S.A. *Journal of Seismic Exploration*, 21: 105-123.

An oil producing limestone reservoir of Wolfcampian age in the eastern shelf of the Permian Basin, Texas is characterized through simultaneous impedance inversion. The spatial distribution of Moran limestone is estimated from P-wave and S-wave (I_P and I_S) impedance volumes, from which V_P/V_S and Lamé attribute ($\lambda\rho$ and $\mu\rho$) volumes are derived. I_P alone will not distinguish limestone from sandstone within the study area. V_P/V_S and I_P attributes from the simultaneous inversion will distinguish limestone from sandstone and shale, and allow estimates of oil saturations. The Lamé parameter attributes also identify lithology and indicate oil saturations. A vertical section through a potential reservoir area predicts oil saturation grading vertically toward the top of the reservoir, and also in the updip direction. The results also show the effect of a water flood within the producing field and other potential oil-saturated limestone reservoirs missed by previous exploration. The main conclusion is that the ($\lambda\rho$ and $\mu\rho$) attributes previously used for analysis of gas reservoirs in clastics are equally valuable for oil reservoirs in carbonates.

KEY WORDS: seismic inversion, carbonates, calibration, 3D, Lamé parameters.

0963-0651/12/5.00

INTRODUCTION

The Permian Basin is one of the most prolific oil provinces in the United States. It has produced over 14 billion barrels of oil (Ball, 1995). It has been heavily explored and is considered to be a mature basin; economic accumulations of hydrocarbons have become increasingly more difficult to find. Despite this difficulty, undiscovered reserve estimates of over 3.5 billion barrels of oil, continue to drive exploration efforts.

Amplitude variation with offset (AVO) inversion is a widely used prospect interpretation and risk reduction tool. While AVO inversion is well developed and somewhat successful in application to porous clastic reservoirs, its application to carbonate reservoirs continues to be less well understood, primarily because the complexity of carbonate diagenesis complicates the relationships between carbonate petrophysical properties and their AVO responses (Li and Downton, 2000; Li et al., 2003b). There are also concerns as to the useability of Gassmann's equations for the seismic modeling of fluid substitution in carbonate reservoirs (Li et al., 2002) because pore connectivity is highly variable in carbonates, and fractures produce anisotropy and macroscopic heterogeneity (Baechle et al., 2005).

Lithology may be distinguished by the relationship between Poisson's ratio and velocity. Li and Downton (2000) show that $\mu\rho$ is a useful indicator of porosity (where μ is the shear modulus, and ρ is density). Much of the current research on AVO for carbonates concerns the distinction between water and gas saturated regions of a reservoir, while little seems to be available concerning the effect of oil, although the AVO effect generalizes and will be sensitive to hydrocarbon density,whether oil or gas is specifically present. King (1966) suggests that V_P/V_S might be sensitive to oil. His lab data show that V_S increases slightly with the replacement of water by liquid hydrocarbons such as kerosene, rather than remaining completely unaffected by the pore fluids. The slight increase in V_S is likely to be caused by a decrease in density. This study attempts to understand the oil signature in limestone reservoirs by interpretive analysis of the P- and S-impedances inverted simultaneously from data from a known oil-producing field in the Permian Basin.

THE STUDY AREA

The eastern shelf of the Permian Basin, west Texas (Fig. 1a) is a platform that developed along the margin of the rapidly subsiding Midland basin during Late Pennsylvanian and Early Permian times (Galloway and Brown, 1973). During the Permian Virgilian and Wolfcampian epochs, a late Paleozoic first-order sea level fall caused approximately 900 m of nonmarine and marine

siliciclastic and carbonate sediments of the Cisco Group to be deposited along the shelf margin (Yang and Kominz, 2002). The shelf prograded ~200 km basinward by accumulation of lowstand deltaic systems and aggraded ~400 m mainly by the growth of shelf-edge carbonate banks (Brown et al., 1987). Sixteen depositional sequences are identified within the Cisco Group; these deposits contain thick shales, conglomeritic sandstones, thin limestones, and some coal (Moore and Plummer, 1922).

The exploration target is the limestones of the Moran Formation of the Cisco Group, which contain large oil reservoirs (Nelson, 1987). Well logs through the producing limestone reservoir indicate that oil is trapped near an updip pinchout; the greatest production is within porosity developments greater than 8% (personal communication with the current operator). This limestone has 3 to 15% porosity and 0.1 md to 54 md permeability which makes it a viable reservoir; the reservoir is draped by sandstone that locally contains small amounts of oil, but has low (1 - 8%) porosity (1982 core report acquired from current operator, Jack Neff). The sand is characteristically limey and very tight, with very low permeability, and so is an effective, but not perfect, seal (J. Carlile, personal communication, 2009).

SEISMIC DATA ACQUISITION

The 3D seismic survey data used (Fig. 1b) cover approximately 114 km^2 (44 square miles) and the largest dimension is oriented parallel to the structural trend. The receiver line spacing was 268.2 meters (880 ft) with a receiver station interval of 60.9 meters (200 ft) and each receiver station has an array of six geophones over 33.5 meters (110 ft). A brick pattern of vibrator lines are perpendicular to the receiver lines, with four vibrators per source point. The source line spacing is 402.3 meters (1320 ft) with a source interval of 67 meters (220 ft). There are a total of 49 receiver lines and 63 source lines.

DATA PROCESSING AND CONDITIONING

The data are processed to increase the signal-to-noise ratio, while maintaining the true relative amplitudes. The processing flow includes a geometry quality check, a 60 Hz filter to remove electrical high line interference, spherical divergence correction,and a surface-consistent spiking deconvolution using a 200 ms operator length to help recover high frequencies, reduce multiples, and produce a close-to-zero-phase output wavelet. Refraction and residual statics and a wavelet transform filter are applied to reduce noise. Non surface-consistent static corrections are applied within each CMP by correlating each trace with a pilot trace calculated for that CMP.

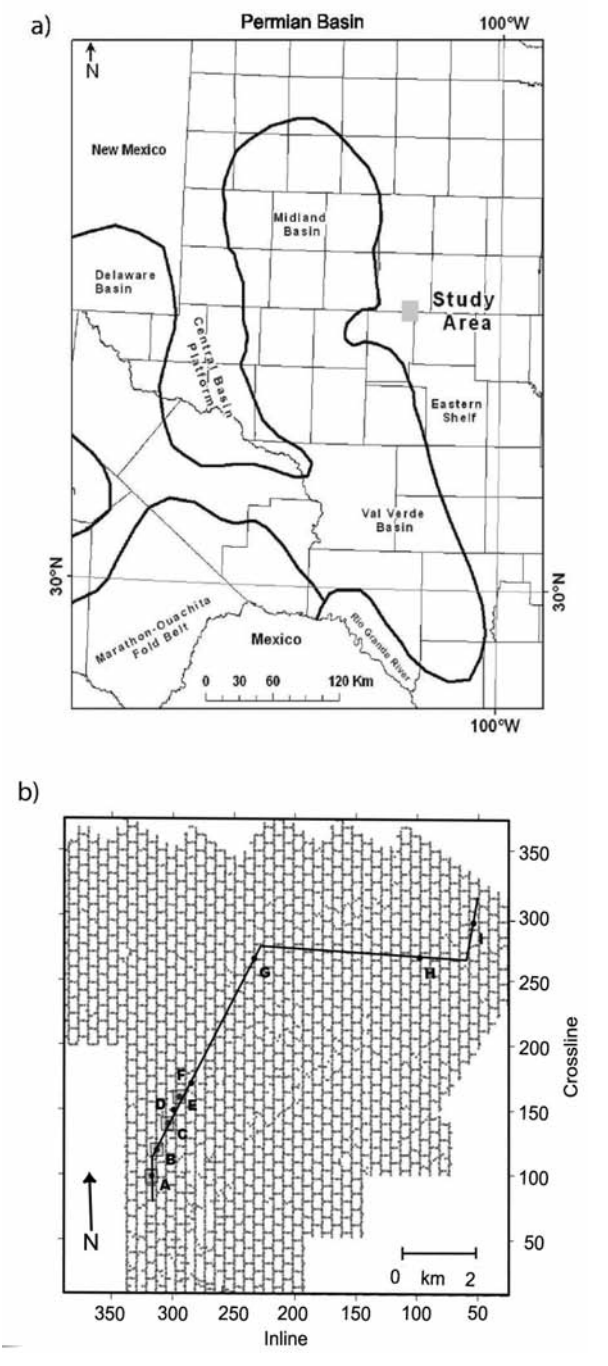

Fig. 1. (a) Structural setting of the study area (the shaded rectangle) on the western edge of the eastern shelf of the Permian Basin. Modified from Silver and Todd (1969). (b) Acquisition geometry. Labeled dots are the well locations used in this study. Boxes around the wells A, B, C, and E indicate the bins used for calibration for simultaneous inversion. Vertical lines contain receivers and horizontal lines contain sources. The solid line through the wells is the swath line.

The effect of the premigration steps is evaluated by comparing the stacked sections before and after their application to the data, a representative X-line section is shown in Fig. 2. A migration velocity analysis is performed on an 0.804 km (0.5 mile) grid spacing, followed by a Kirchhoff prestack time migration.

The simultaneous inversion uses common-angle gathers, and these data needed to be conditioned to optimize the inversion. Low frequency noise is reduced using adaptive, time-variant subtraction, followed by residual normal moveout corrections (R_{NMO}). Random noise was further reduced by muting beyond the 0-48 degrees incident angle range. Supergathers are generated using a mean average rolling window of three X-lines and three Inlines. A stack of the supergathers is generated to estimate a wavelet and also to correlate the well logs to the seismic data. The correlation is performed and three common-angle gather stacks (0°-15°, 15°-30°, and 30°-45°) are generated for input to the inversion. Figs. 3a and 3b show three representative CMP gathers before and after conditioning, respectively; conditioning consisted of noise reduction, R_{NMO}, and muting. Fig. 3c contains the angle gathers from the supergathers at the same Inline positions.

WELL LOGS AND CALIBRATIONS

There are many wells drilled in the area; almost all have gamma and resistivity logs and either a neutron density or sonic log. Because of the concentrated well spacing, correlation of interwell lithology was straightforward using gamma logs (Fig. 4). Because S-wave logs were not available, they needed to be approximated for the low frequency background model for input to the simultaneous inversion (the simultaneous elastic inversion subsequently estimates the higher frequency variations of both P- and S-wave impedances and density). Castagna et al.'s (1993) mudrock equation was used to estimate shear-wave velocity logs for wet sand and shale from P-wave logs. The focus of this study is a limestone reservoir, so the mud-rock line equation will not be valid within the limestone zone. Separate calibrations are required for the clastic and the carbonate portions of the section (Li et al., 2002; 2003a,b). The empirical Greenberg and Castagna (1992) equation was used within the limestone depth range. This calibration defines the constraints that are subsequently applied during inversion of the input seismic and well log data. The main condition for an acceptable calibration is that it produce reliable predictions of the known seismic impedances at the wells for which the calibrations were done. The final inversion is performed for I_P, I_S, and ρ over the entire seismic data volume, and is interpreted for lithology and fluids.

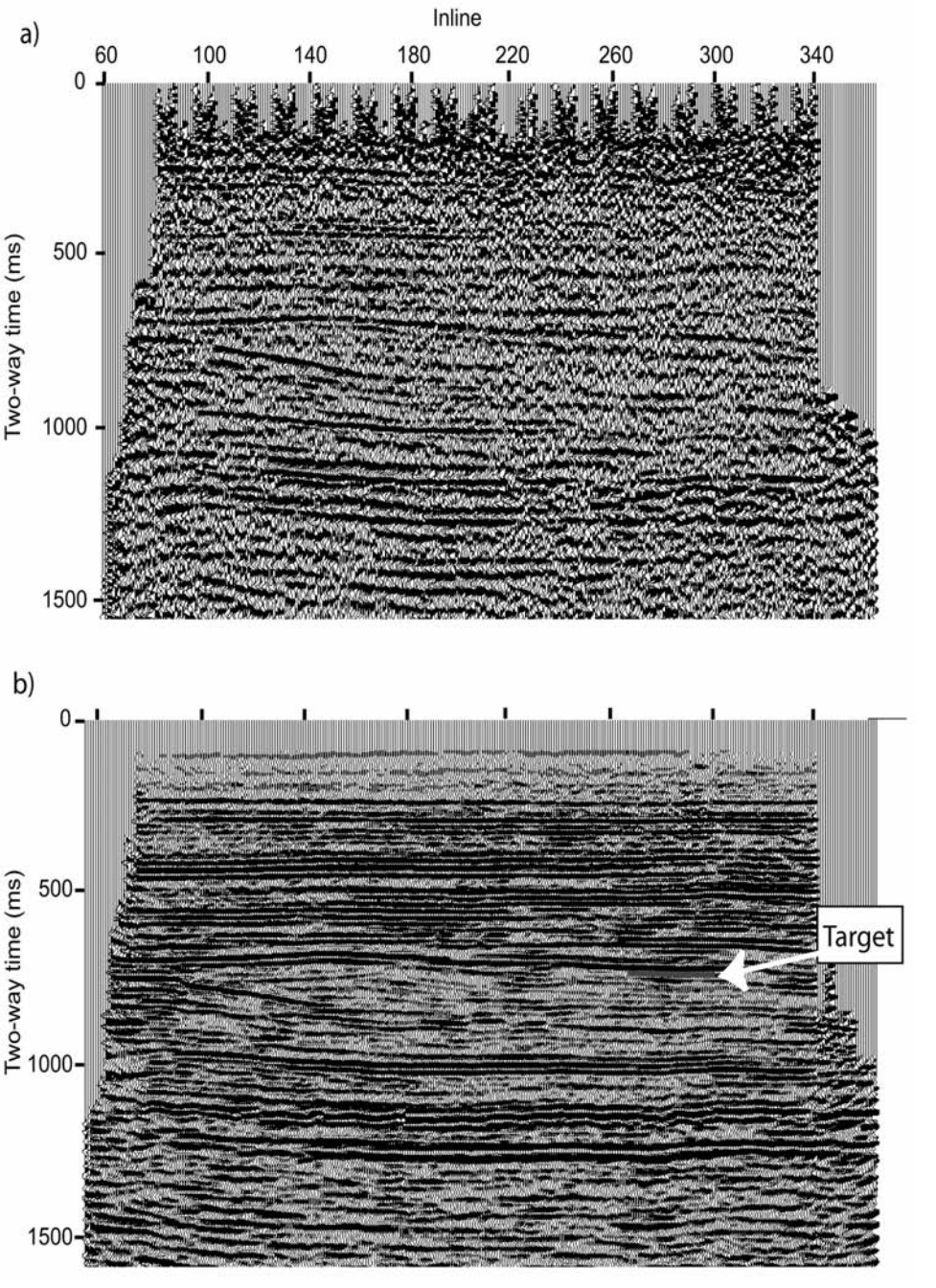

Fig. 2. Brute stack before (a) and after (b) data processing. This section is along X-line 164. The arrow n in (b) points to the location of the known limestone reservoir. The separation between the Inline locations is 110 ft (33.5 m).

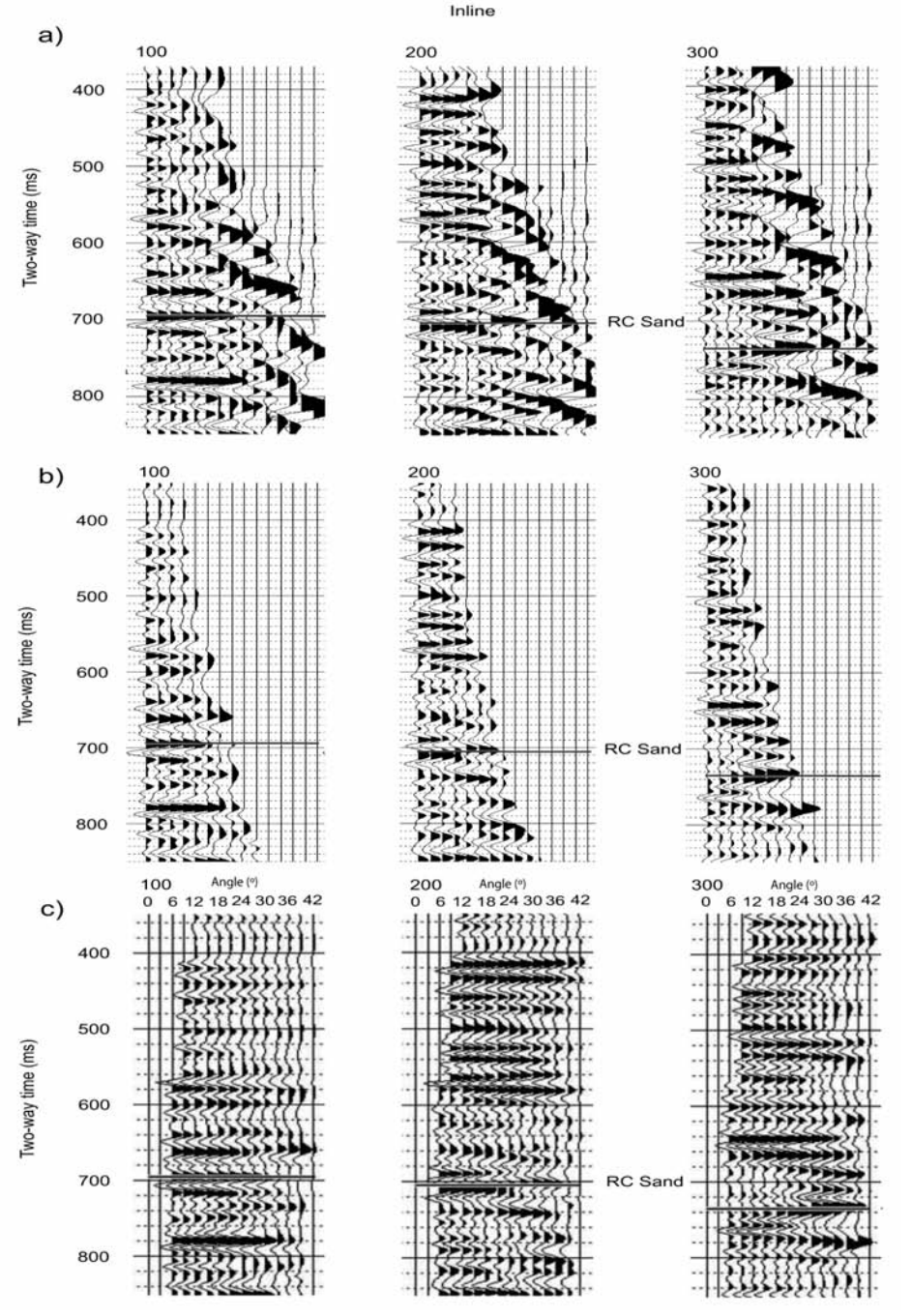

Fig. 3. CDP gather conditioning for simultaneous inversion. The RC Sand horizon is the sand marker right above the target Moran limestone reservoir. (a) shows representative CDPs at Inlines 100, 200 and 300, prior to conditioning; (b) are the same CDPs after noise reduction, muting, and R_{NMO} correction are applied. (c) are the angle gathers from the supergathers at the same three Inline positions. These gathers are all on X-line 190.

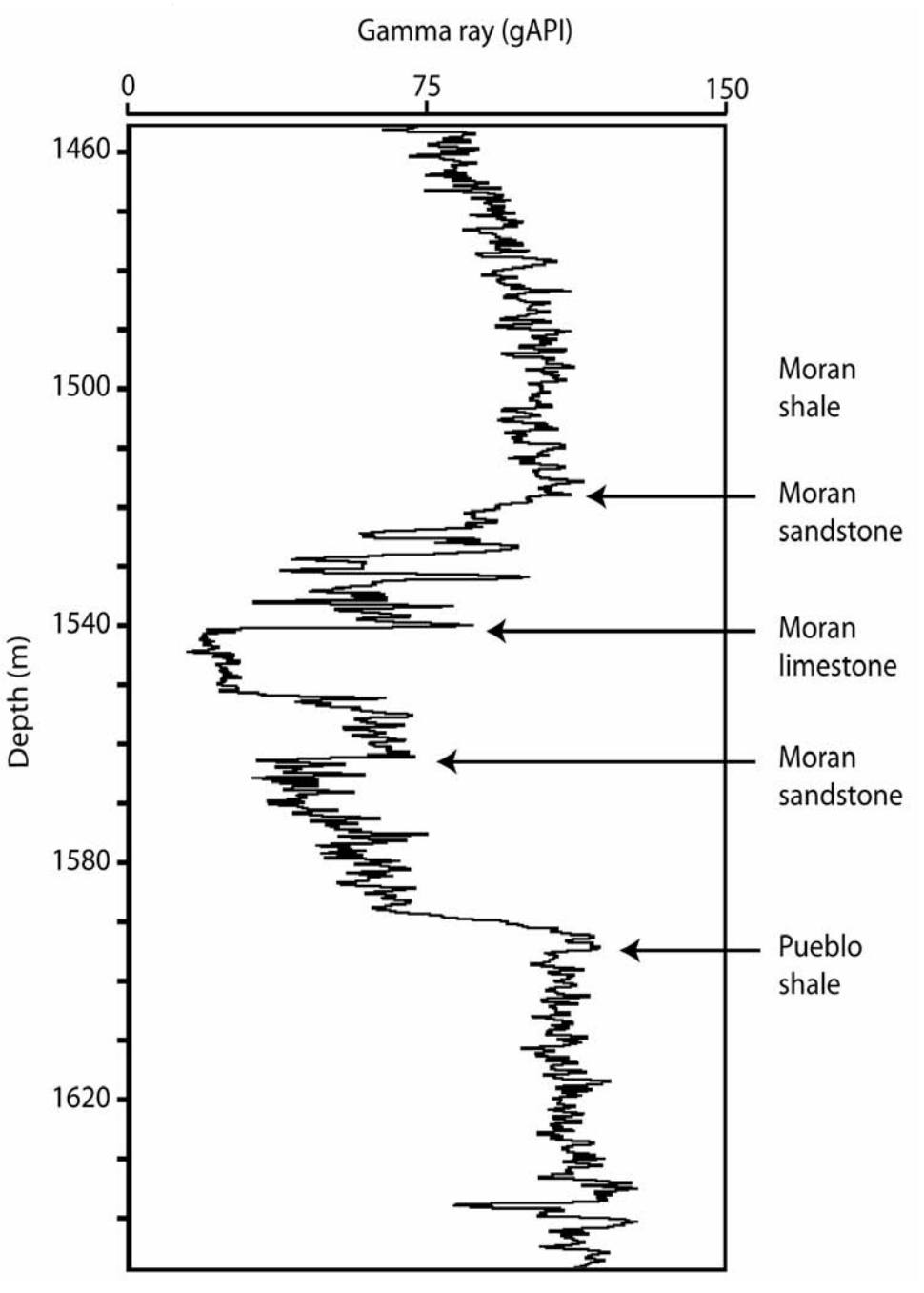

Fig. 4. Gamma log from well E, through the reservoir; arrows indicate formation tops.

INVERSION

Pre-stack simultaneous inversion produces estimates of P-impedance, S-impedance, and density (I_P, I_S, and ρ) from reflection coefficients as a function of angle, assuming that the logarithms of I_P, I_S, and ρ, are linearly related (Hampson et al., 2005). We use prestack time-migrated common-angle gathers as input and constraints from well logs to stabilize, and reduce the non-uniqueness of the inversion.

A separate wavelet estimation is done for each of three common-angle gather stacks. Time-dependent bounds on the P-wave velocity, S-wave velocity and density are defined for the inversion. Four wells (A, B, C, and E in Fig. 1b) that penetrated the reservoir, and have sonic and density logs, are used for calibration. The cross plot of the gamma and I_P values (calculated from the sonic and density logs of the four calibration wells) in Fig. 5 clearly shows that acoustic impedance alone will not distinguish limestone from sandstone within this area. The gamma values separate the plot into shale, sandstone, and limestone regions (Fig. 5b). The crossplot indicates that shale can be distinguished from limestone as their I_P values do not overlap (Fig. 5), but this is not always true. For example, Li et al. (2003b) show, in data from the Western Canada Sedimentary Basin, that I_P is insufficient to separate shale from the effects of porosity in a carbonate.

Historical production reports (https://penerdeq.ihsenergy.com) indicate a very low gas-oil-ratio (GOR) within the limestone reservoir, so the seismic velocity changes over time are to be associated with oil replacement by brine, rather than changes in gas content. The main difference between this study and previous ones, is that the main reservoir hydrocarbon is oil rather than gas.Thus, the model is assumed to be a reservoir with two fluid components, brine and oil. Wells C and E (Fig. 1b) were shut-in at the time the seismic survey was shot, and well B was plugged as wet, so water saturation was assumed to be near 100% for these wells. Well A was producing when the seismic survey was shot and was modeled at 50% water saturation, from the production records (https://penerdeq.ihsenergy.com).

LITHOLOGY DETERMINATION USING LAMÉ PARAMETERS

The I_P and I_S data volumes can be used to derive two Lamé attribute volumes ($\lambda\rho$ and $\mu\rho$) which can often be good indicators of changes in pore fluids and lithologic properties (Goodway et al., 1997; Yi et al., 2003a,b). The relationships of the Lamé attributes to I_P and I_S are

$$\lambda\rho = I_P^2 - 2I_S^2 \ , \tag{1}$$

and

$$\mu\rho = I_S^2 \ . \tag{2}$$

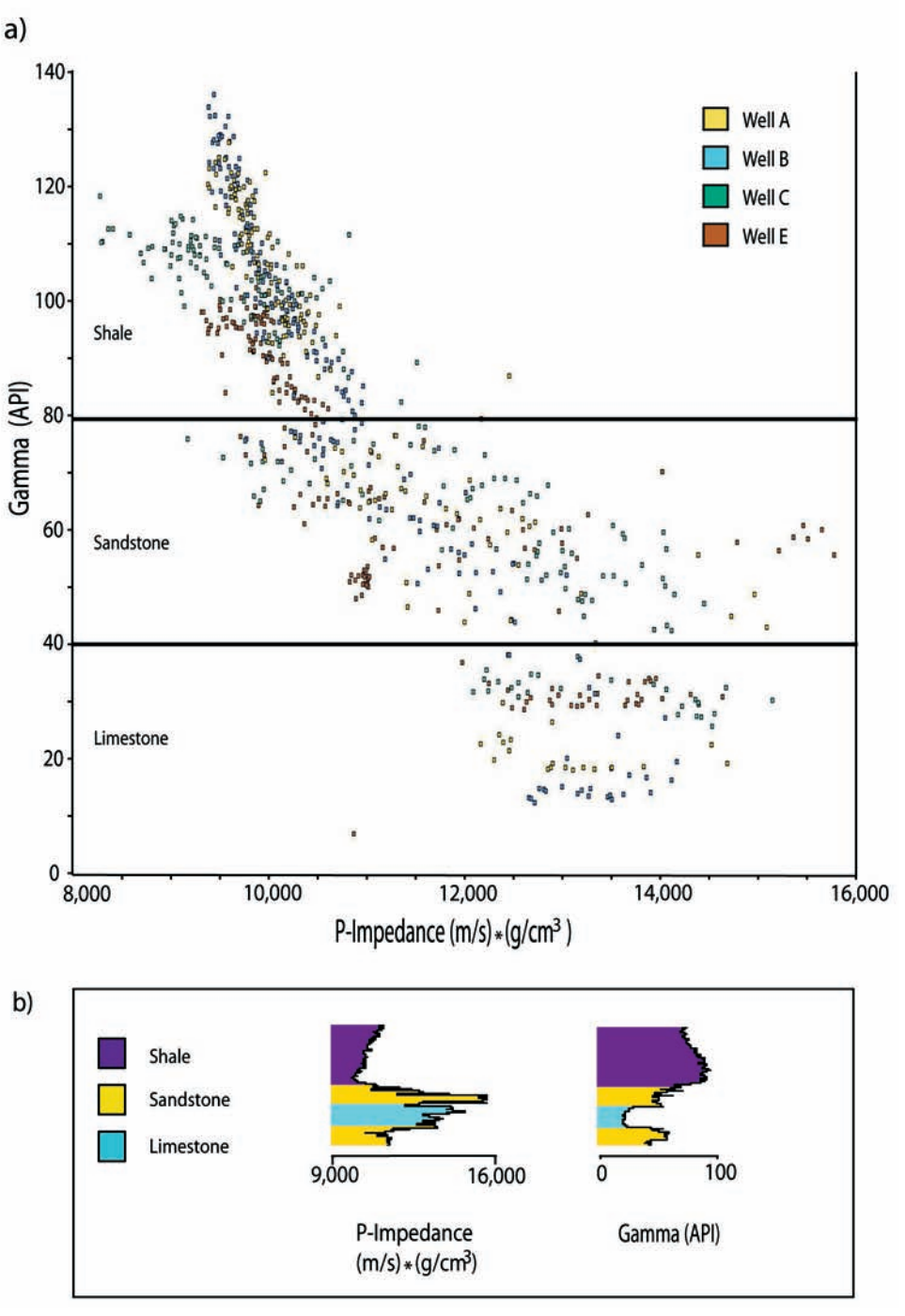

Fig. 5. Gamma vs. P-impedance crossplot from logs from wells A, B, C, and E. (a) shows lithology separation and P-impedance overlap for sandstone and limestone. (b) shows the P-impedance and gamma to display the lithology regions around the target limestone in well E.

The Lamé parameters are incompressibility λ (which is sensitive to the pore fluids), and the rigidity μ (which is the shear modulus and independent of the pore fluid) (Goodway et al., 1997). The crossplot in Fig. 5 shows how the relationship between $\lambda\rho$ and $\mu\rho$ change with respect to lithology and to oil saturation of the limestone. The crossplot uses the same wells (A, B, C, and E) and the oil saturation estimates from the production data, as described above.

There are two steps to compute the Lamé attributes within the limestone reservoir at the calibration wells. The first step is to estimate the I_P and I_S logs from the P-wave, S-wave [computed from the Greenberg and Castagna (1992) equation], and density logs. Using these I_P and I_S values, $\lambda\rho$ and $\mu\rho$ logs were estimated using eqs. (1) and (2). The data ranges and trajectories in Fig. 5 are similar to those in Figs. 1 and 4 of Li et al. (2002), and in Fig. 5C of Li et al. (2003a,b).

In the second step, fluid replacement modeling is performed for well A to show the distribution of Lamé attributes ($\lambda\rho$ and $\mu\rho$) with varying oil saturation from 0 - 100%. The crossplot of the Lamé attributes $\lambda\rho$ and $\mu\rho$ from the simultaneous inversion within a 15 ms time window below the bottom of the Moran sandstone (to correspond to the carbonate), Fig. 6 shows a clear separation of limestone from the sand-shale background. This is consistent with the previous observations by Li et al. (2002, 2003a,b). The limestone falls in a small $\lambda\rho$-$\mu\rho$ region, within which the position of each point depends on oil saturation. The resulting estimate of the horizontal extent of the limestone matches well with the corresponding estimate from V_P/V_S (not shown).

FLUID DETERMINATION USING LAMÉ PARAMETERS

Li and Downton (2000) indicate that if water is replaced by gas, there will be a decrease in $\lambda\rho$, and $\mu\rho$ remains relatively unaffected, assuming that porosity is constant. Rafavich (1984) shows, in dolomite data, that the effects of decreasing fluid density on $\lambda\rho$, $\mu\rho$, P-velocity, and V_P/V_S are detectable using seismic data. $\lambda\rho$ decreases because it is the product of incompressibility and density. Less information is available for oil saturation (King, 1966), but both oil and gas have a lower incompressibility than water and both are also less dense, causing the bulk density to decrease; thus $\lambda\rho$ decreases with the replacement of water by a less dense (hydrocarbon) fluid; $\mu\rho$ is less affected because the shear modulus μ is less affected by fluids than λ is.

The Lamé attributes $\lambda\rho$ and $\mu\rho$ from the simultaneous inversion are extracted and crossplotted (Fig. 6); all data that fell within the Lamé attribute limestone region are plotted as the corresponding oil saturation in Fig. 7. As expected, $\mu\rho$ changes less than $\lambda\rho$ as oil saturation changes from 0 to 100%.

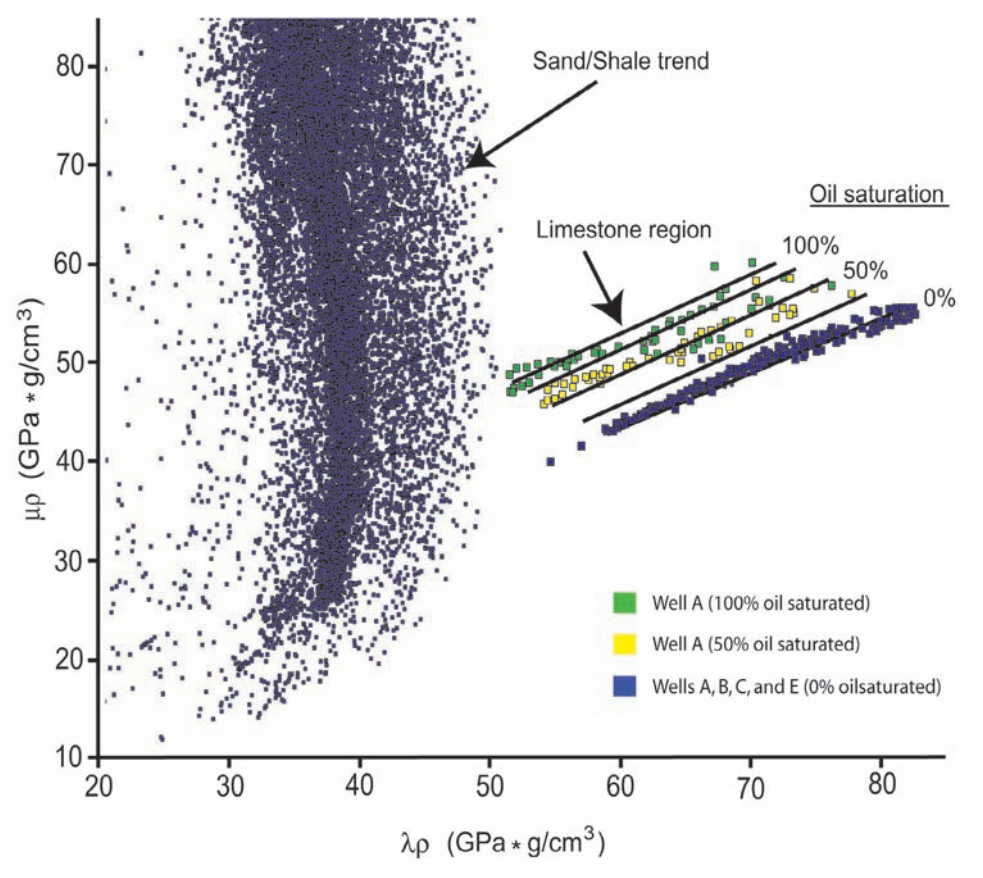

Fig. 6. $\lambda\rho$ vs. $\mu\rho$ crossplot of data from logs from wells A, B, C, and E. This shows the separation of limestone from the shale/sandstone trend and the changes in $\lambda\rho$ and $\mu\rho$ in well A as oil saturation increases from 0 to 100%. Saturation was estimated by fluid substitution with the Gassmann equation, for a representative porosity of 10%.

INTERPRETATION

In the map in Fig. 7, the colors show the distribution of the oil saturation within the limestone, as estimated from $\lambda\rho$ and $\mu\rho$ (Fig. 6). $\lambda\rho$ and $\mu\rho$ are more sensitive to fluid changes than V_P and V_S (Castagna et al.,1993; Goodway et al., 1997). Wells A, B, C, E, and F are drilled through the limestone reservoir. This field has been under water flood since 1991 (12 years before the seismic survey was shot), and explains our results which show low oil saturations

around these wells (Fig. 7). There is exploration potential within the adjacent southern and eastern portions of the field where there is greater estimated oil saturation. The limestone to the north of the producing reservoir has less potential because the limestone is less continuous. The northeast-southwest trend of limestone along the eastern flank of the survey show connectivity and high estimated oil saturations and thus appear to have good exploration potential.

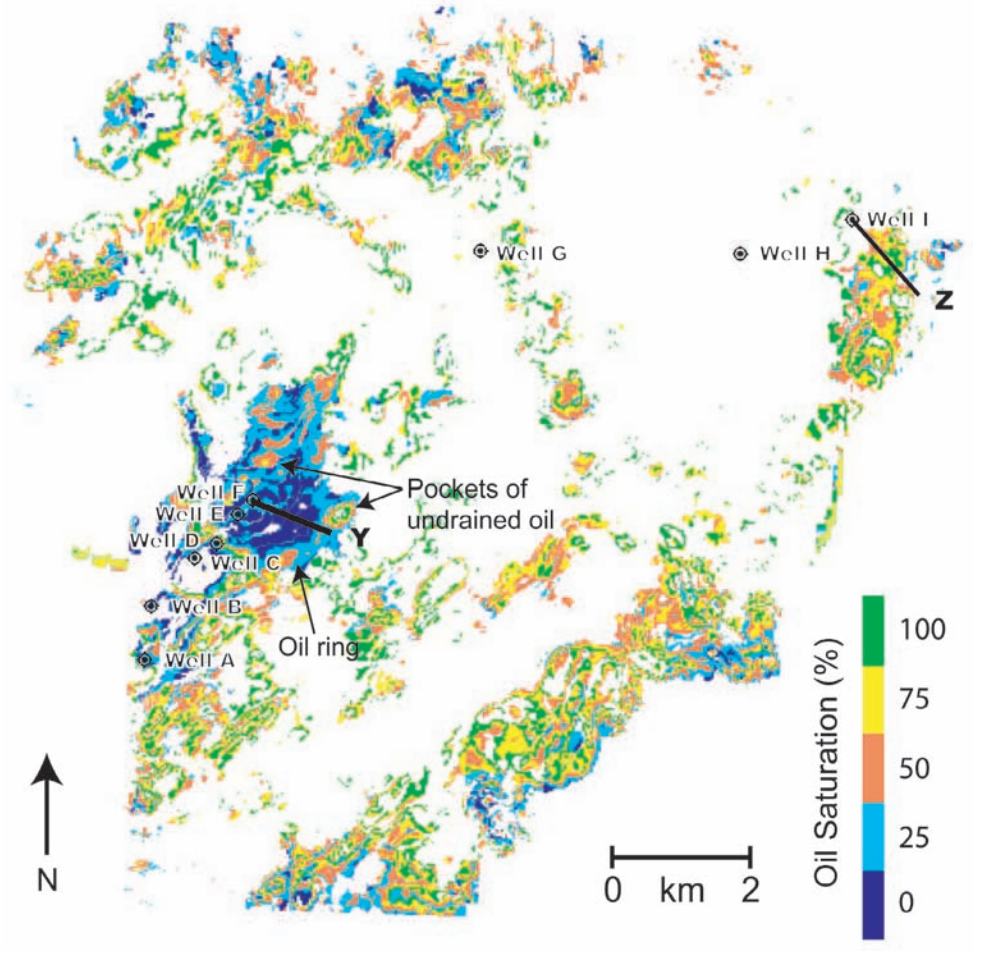

Fig. 7. Map of the predicted limestone distribution, colored with oil saturation estimated from $\lambda\rho$ vs. $\mu\rho$. The white portions are sands or shales, or are outside of the survey boundaries.

Plots of V_P/V_S, I_P, $\lambda\rho$, $\mu\rho$, and oil saturation obtained via the $\lambda\rho$ and $\mu\rho$ crossplot are generated for representative vertical slices through both the known limestone reservoir, and a prospective location. These attribute slices are plotted together for comparison (Figs. 8 and 9). The water-flooded limestone reservoir slice, (along line Y in Fig. 7) shows a V_P/V_S ratio (Fig. 8a) of $\sim$1.85 (blue) which is consistent with Domenico's (1984) water saturated limestone range of 1.84 to 1.99. The I_P in the carbonate (Fig. 8b) is within the sandstone - limestone I_P range 11887 (m/s)*(g/cm^3) to 15240 (m/s)*(g/cm^3) (Fig. 5). The $\lambda\rho$ section (Fig. 8c) shows a slight decrease (blue to red) moving from west to east and moving updip in the limestone reservoir, while the $\mu\rho$ section (Fig. 8d) appears relatively constant (yellow). The corresponding estimated oil saturation (Fig. 7e) section indicates an increase of oil in the updip part of the section, and also shows two spots that suggest oil-filled compartments in the limestone that have been bypassed, by both the primary production, and by the water-flooding. In Figs. 8e and 9e, only the voxels that strictly satisfy both the reservoir lithology and minimum hydrocarbon content are plotted in color; the blocky appearance is a consequence of the low resolution of the oil saturation (Fig. 6) and the limitation of the 2 ms sampling of the original seismic data.

For the prospective location (line Z in Fig. 7), the vertical V_P/V_S slice (Fig. 9a) shows the interpreted limestone reservoir to have a V_P/V_S range between 1.80 to 1.90. This reduction in V_P/V_S ratio from the water bearing limestone section, in Fig. 8a, is similar to the gas effect as described by Tatham and Stoffa, (1976) and Li and Downton, (2000), and is related to the increase in oil saturation, by the replacement of water by a less dense fluid. The I_P section (Fig. 9b) is consistent with the sandstone - limestone I_P range shown in Fig. 5. The $\lambda\rho$ section (Fig. 9c) shows a decrease in value from the water bearing limestone in Fig. 8c, and $\mu\rho$ (Fig. 9d) is fairly constant from west to east until X-line 280, where it increases slightly. The estimated oil saturation (Fig. 9e) not only indicates an increase in oil saturation, but shows saturation grading vertically with higher oil saturation on top of lower oil saturation, which is the expected effect of gravity.

In summary, the relationships between V_P/V_S and I_P and between $\lambda\rho$ and $\mu\rho$ provide direct hydrocarbon indicators for the potential exploration of new reserves and also the monitoring of a water-flood. The limestone oil saturation map predicts a ring of higher oil saturation around the eastern edge of the water flood in the interpreted reservoir (Fig. 7), and also small pockets of oil which have not been drained (Fig. 8e).

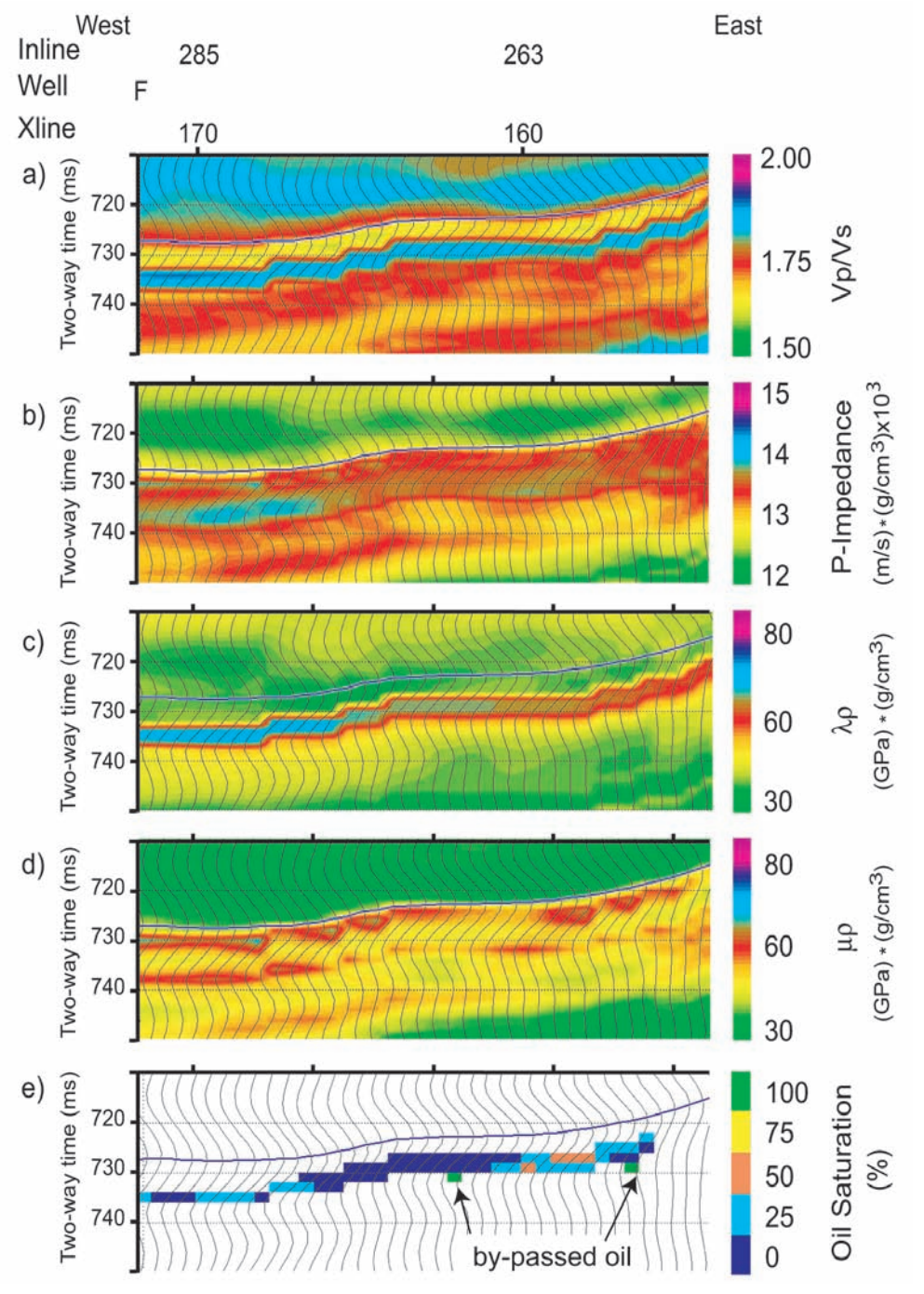

Fig. 8. Section through the known, water-flooded, limestone reservoir. The location of this line is marked Y in Fig. 7. (a) V_P/V_S, (b) I_P, (c) $\lambda\rho$, (d) $\mu\rho$, (e) oil saturation based on the crossplot of $\lambda\rho$ vs. $\mu\rho$ in Fig. 6. The separation between Inline points in the Inline direction, and between X-line points in the X-line direction, is 110 ft (33.5 m).

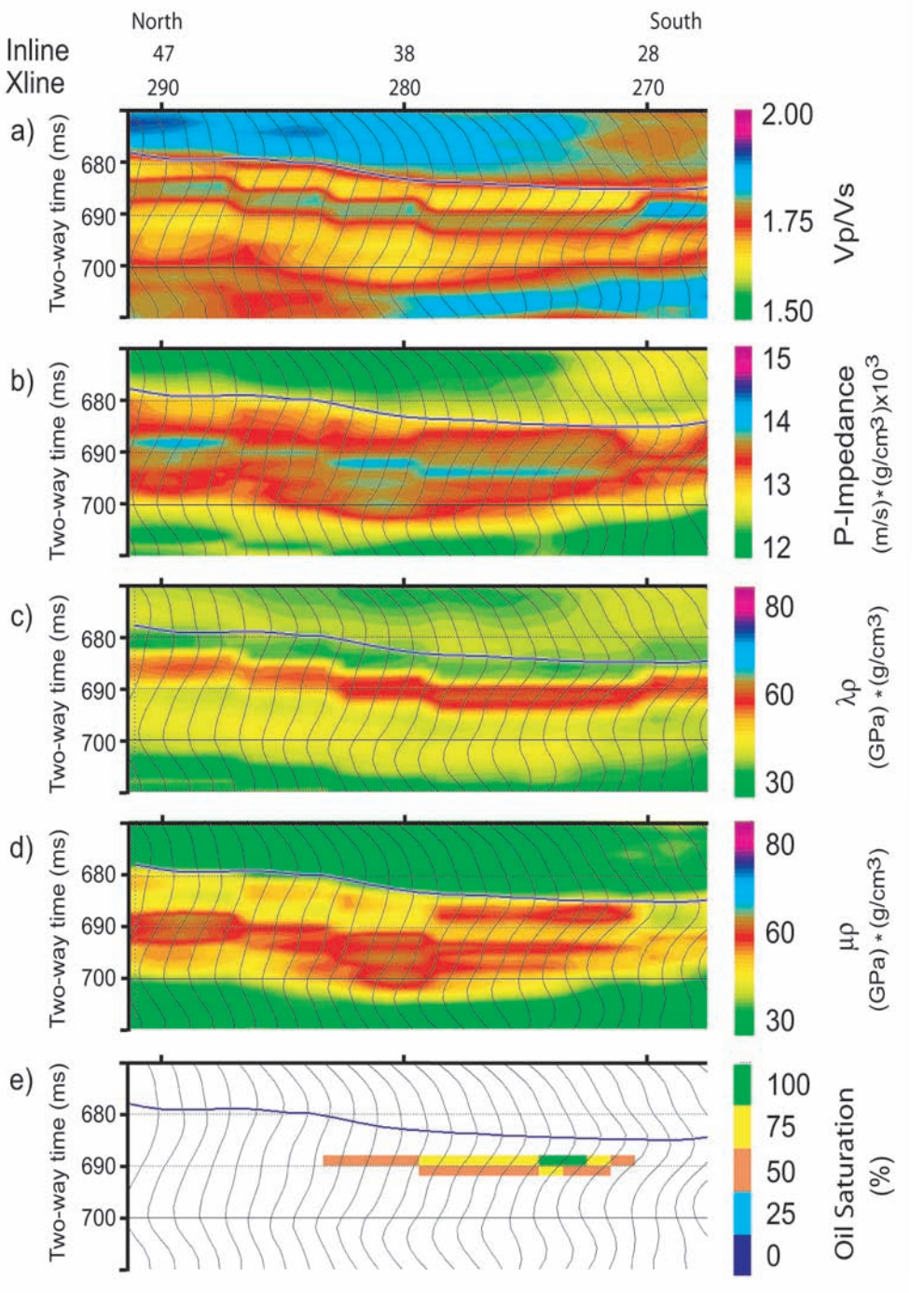

Fig. 9. Section through prospective limestone reservoir (line Z in Fig. 7), showing high oil saturations. (a) V_P/V_S, (b) I_P, (c) $\lambda\rho$, (d) $\mu\rho$, (e) oil saturation based on the crossplot of $\lambda\rho$ vs. $\mu\rho$ in Fig. 6. The separation between Inline points in the Inline direction, and between X-line points in the X-line direction, is 110 ft (33.5 m).

DISCUSSION

Limitations associated with the input data that influence the results, include the distribution of control wells, the types and number of well logs available for calibration, the timing of drilled wells and logging relative to the seismic data acquisition, the reservoir fluid characteristics, and the available range of incident angles for the seismic impedance inversions. Limitations associated with the interpretation include differences in data coverage near the survey edges, the location and distribution of validation wells for the interpretation, and the validity of Gassmann's equations for fluid replacement in carbonates, and the associated uncertainties (Engelmark, 2002).

There are only four wells available with both sonic and density logs (A, B, C, and E), that are drilled through the known reservoir. Consequently, there are large regions of the survey with no direct well calibration for the inversion. Three of the four wells (A, B, and E) are drilled and logged 21-36 years before the seismic was shot, so fluid saturations at the time of the survey had to be estimated from production reports. The simultaneous inversion assumed software default values of bulk modulus and density of the fluids because fluid properties are not directly known. The density estimate from the simultaneous inversion is less reliable than the impedance estimates (I_P, and I_S) because the reflection angle aperture was limited to 48°. Some of the most prospective areas (Fig. 7) are near the survey edge and so have reduced seismic data coverage. Validation of the interpretation is limited to wells within the known reservoir because there are no wells drilled yet through the identified prospective areas. An increase in $\mu\rho$ values for fluid replacement at the calibration wells (A, B, C, and E), questions the validity of using Gassmann's equations for fluid replacement within carbonates.

Future simultaneous inversions can be done in adjacent areas of the Permian Basin, as the present study demonstrates feasibility. Potential for other Moran limestone reservoirs exist in the area, as well as shallower and deeper carbonate reservoirs, such as the fractured dolomites of the Merkel Formation of the Clear Fork Group, or the karsted dolomites of the Ellenberger Formation. This technology can be also be applied to the clastics to differentiate sandstones from shale and to identify areas where reservoirs are vertically stacked, to enhance exploration potential and to improve production economics.

This study focuses on the characterization of the limestone component of the producing field. The study also revealed information on the water flood within the limestone reservoir which began in 1991 (https://penerdeq.ihsenergy .com). Comparison of the map in Fig. 6, with the water flood strategy, would help evaluate the results.

SUMMARY

We perform simultaneous impedance inversion of 3D seismic land survey data from the eastern shelf, Permian Basin, Texas. The modulus attributes $\lambda\rho$ vs. $\mu\rho$, previously applied in other studies to evaluate gas reservoirs in clastics, are also applicable to oil reservoirs in carbonates. The objectives in the present study are to image the known producing Moran limestone reservoir, to estimate oil saturation, and to locate other reservoirs with high oil saturations that have not been previously known, or were missed by previous drilling. I_P alone will not distinguish limestone from sandstone within the area. V_P/V_S vs. I_P, and $\lambda\rho$ vs. $\mu\rho$, which are estimated from I_P and I_S, are able to discriminate sandstone from limestone and are the basis for estimation of oil saturation within the limestone.

Analysis of the inverted attributes suggests that there are other viable limestone oil reservoirs within the study area. Characterization of one such potential reservoir shows an increase of oil saturation grading vertically toward the top of the reservoir, and also in the updip direction. Characterization of the producing limestone reservoir shows high water saturations where the field was water flooded, and additional drilling potential to the southeast of the field. We found simultaneous impedance inversion to be a useful technology for direct hydrocarbon detection, monitoring of water-floods, and predicting previously passed-over reserves in the study area. Validation of the predictions made in this study can be done only by drilling.

ACKNOWLEDGMENTS

The research leading to this paper was supported by the Sponsors of the UT-Dallas Geophysical Consortium.The seismic data were provided by Bright and Co. The inversions were done using Hampson-Russell STRATA software. We thank Becky Buehner at Geotrace for the pre-inversion processing of the seismic data, and the support staff at Hampson-Russell for providing answers to many questions. This paper is Contribution No. 1227 from the Department of Geosciences at the University of Texas at Dallas.

REFERENCES

Ball, M., 1995. Permian Basin Province (044). In: Gautier, D.L., Dolton, G.I., Takahashi, K.T. and Varnes, K.L. (Eds.), 1995, National Assessment of United States Oil and Gas Resources-results, Methodology, and Supporting Data. U.S. Geological Survey Digital Data Series DDS-30.

Baechle, G.T., Weger, R.J., Eberli, G.P., Massafero, J.L. and Sun, Y., 2005. Changes of shear moduli in carbonate rocks: Implications for Gassmann applicability. The Leading Edge, 24: 507-510.

Brown, L.F., Iriarte, R.F.S. and Johns, D.A., 1987. Regional stratigraphic cross sections, Upper Pennsylvanian and Lower Permian strata (Virgilian and Wolfcampian Series), north-central Texas. The University of Texas at Austin, Bureau of Economic Geology Cross Sections.

Castagna, J.P., Batzle, M.L. and Kan, T.K., 1993. Rock physics-The link between rock properties and AVO response. In: Castagna, J.P. and Backus, M. (Eds.), Offset-dependent Reflectivity - Theory and Practice of AVO Analysis. Investigations in Geophysics, No. 8, SEG: 135-171.

Engelmark, F., 2002. Error propagation in Gassmann modeling for 4D feasibility studies. The Leading Edge, 22: 984-987.

Galloway, W.E. and Brown, L.F., 1973. Depositional systems and shelf-slope relations on cratonic basin margin, uppermost Pennsylvanian of north-central Texas. AAPG Bull., 57: 1185-1218.

Goodway, W., Chen, T. and Downton, J., 1997. Improved AVO fluid detection and lithology discrimination using Lamé petrophysical parameters; "$\lambda\rho$", "$\mu\rho$", & "λ/μ fluid stacks", from P- and S-inversions. Expanded Abstr., 67th Ann. Internat. SEG Mtg., Dallas: 183-186.

Greenberg, M.L. and Castagna, J.P., 1992. Shear-wave velocity estimation in porous rocks: Theoretical formulation, preliminary verification and applications. Geophys. Prosp., 40: 195-209.

Hampson, D.P., Russell, B.H. and Bankhead, B., 2005. Simultaneous inversion of pre-stack seismic data. Expanded Abstr., 75th Ann. Internat. SEG Mtg., Houston: 1633-1637.

King, M.S., 1966. Wave velocities in rocks as a function of changes in overburden pressure and pore fluid saturants. Geophysics, 31: 50-73.

Li, Y. and Downton, J., 2000. The application of amplitude versus offset in carbonate reservoirs: Re-examing the potential. Expanded Abstr. 70th Ann. Internat. SEG Mtg., Calgary, Alberta: 166-169.

Li, Y., Downton, J. and Goodway, B., 2003a. Recent applications of AVO to carbonate reservoirs in the Western Canadian Sedimentary Basin. The Leading Edge, 22: 670-674.

Li, Y., Goodway, B. and Downton, J., 2003b. Recent advances in application of AVO to carbonate reservoirs. CSEG Recorder, 22: 34-40.

Li, Y., Pickford, S., Goodway, B., Downton, J. and Pickford, S., 2002. Recent advances in application of AVO in carbonate reservoirs: calibration and interpretation. Expanded Abstr., 72nd Ann. Internat. SEG Mtg., Salt Lake City: 269-272.

Moore, R. and Plummer, F., 1922. Pennsylvanian stratigraphy of north central Texas. J. Geology, 30: 18-42.

Nelson, R., 1987. Rose Creek (Wolfcamp), Oil and Gas Fields in West Texas Symposium, 4. West Texas Geol. Soc., Public. 87-83: 103-106.

Rafavich, F., Kendall, C.H.S.C. and Todd, T.P., 1984. The relationship between acoustic properties and the petrographic character of carbonate rocks. Geophysics, 49: 1622-1636.

Silver, B.A. and Todd, R.G., 1969. Permian cyclic strata, northern midland basins, west Texas and southeastern New Mexico. AAPG Bull., 53: 2223-2251.

Tatham, R.H. and Stoffa, P.L., 1976. V_P/V_S - A potential hydrocarbon indicator. Geophysics, 41: 837-849.

Tatham, R.H., 1982. V_P/V_S and lithology. Geophysics, 47: 336-344.

Yang, A. and Kominz, M.A., 2002. Characteristics, stratigraphic architecture, and time framework of multi-order mixed siliclastic and carbonate depositional sequences, outcropping Cisco Group (Late Pennsylvanian and Early Permian), Eastern Shelf, north-central Texas, USA. Sediment. Geol., 154: 53-87.